WCTE 2016
World Conference on Timber Engineering
August 22-25, 2016 | Vienna, Austria

CHARACTERIZATION OF THE *HALVED AND UNDERSQUINTED SCARF* CARPENTRY CONNECTION.

Perria Elena[1], Paradiso Michele[2], Kessel Martin[3], Sieder Mike[4]

ABSTRACT: The purpose and behaviour of joints in the structure is very important during the study of a structure. Scarf joints significantly affect the general stiffness of a structure. Very often, the lack of good rational methods in design practice with respect to risk for perpendicular to grain fracture brings to a generalized presence of errors in phase of strengthening or design timber structures. Experimental tests and analytic models for the description of the *halved and undersquinted scarf* are presented. These are the evidence and the basis for the future development of the more complex *splayed and tabled scarf joint with key* behaviour. The description of such carpentry connection is of importance in a scientific field for the knowledge of the mechanical behaviour of old timber systems and many applications in the structural analysis.

KEYWORDS: timber structure, carpentry connection, halved and undersquinted scarf, heritage

1 INTRODUCTION

What it is due to remark on the behaviour of structural joints is that they govern the stress capacity of the whole structure. It is critical that a joint could be able to carry and transmit loads successfully, because they can be a point of weakness (or force) for the structure. The nature of the hand crafted old structures is very uncertain; in first stand, the imperfections are intrinsic with the nature of the workmanship, then the variety of geometries and employed wood, adds unreliability about any certain understanding on the carpentry structures' behaviour. Consequently, in first stand it is appropriate to generally understand the structure and make some specific assumptions about the purpose and behaviour of the joints, because they normally governs the whole strength and stiffness of the structure.
The first step to this overall understanding is the description of the employed carpentry joints behaviour through a static model. This is of importance in a scientific field for the knowledge of the mechanical behaviour of old constructional systems and many applications in the structural analysis with the aim of reinforce and restoration of old timber structures.

1.1 State-of-the-art on the wood-wood connections

The knowledge on the carpentry joints is mainly praxis and know-how based on the good practice of expert carpenters. In the last two decades wood-wood connections has been studied from various researchers and important steps has been done.
Because of his diffusion, design rules for the *mortise and tennon* and also the *notched joints*, have their counterparts in some Spanish and German standards. [4, 5 - 6]. The *lap joints* and the *scarf joints* are also very diffused in original old structures and for their reparation, or in modern structures; nevertheless, the few research campaign have been conducted are not necessary to develop some design or reparation rules. The few research on the *scarf* family focuses on the tensile resistance of the *splayed and tabled scarf with key*, also called *Jupiter joint* [15] and the *halved and table tennoned scarf*, from [1]. About the bending resistance, the study carried out by TRADA [17] suggest that the limiting moment capacity for the *scarf joint* is only equal to one third of the strength of the correspondent unjointed beam. More, an analysis about the bending capacity of various types of scarf and the reinforcing effect of wooden pegs was done by [9].
The present research is demonstrating that the design equations developed for notched beams contained in the EU5 [7, section 8.6.1] and applied for the analysis of some kind of scarf joints are not reliable for the anticipation of the load-bearing behaviour. Furthermore, according with [15], also the approach to the shear resistance of old carpentry joints that refers to standard shear tests for contemporary structures may be not suitable for old

[1] Elena Perria, Università di Firenze & Technische Universität Braunschweig, elena.perria@dicea.unifi.it
[2] Paradiso Michele, Università di Firenze, michele.paradiso@unifi.it
[3] Martin H. Kessel, Technische Universität Braunschweig, m-h.kessel@tu-bs.de
[4] Sieder Mike, Technische Universität Braunschweig, m.sieder@tu-braunschweig.de

structures, because there is expected a non-realistic uniform moisture content and distribution of forces. Some more research is needed.
The generalized presence of wooden frame buildings or part of buildings in the European and North American area, and the relatively numerous developed investigations, have no counterpart in the European and North American codes and regulations for what concerns wooden-wooden connections. The lack of good rational methods in design practice with respect to risk for perpendicular to grain fracture [2] brings to a generalized presence of errors in phase of strengthening or design e.g. overlapping of unsuitable techniques during the remodelling of existing structures, or over-dimensioning of structures in case of new structures.
Because of the variety of all this intrinsic uncertainties, a good understanding of how the joints work and how the forces are balanced is required, in order to develop design and reinforcement specification for joints [3].

2 THE *HALVED AND UNDERSQUINTED SCARF JOINT.*

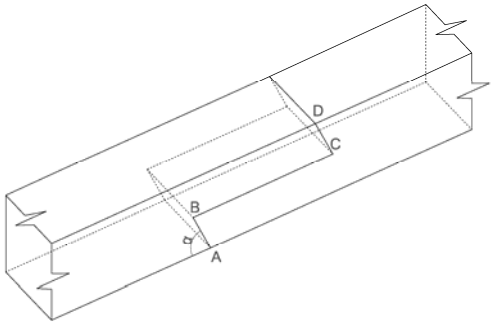

Figure 1: The halved and undersquinted scarf joint

2.1 Geometry, diffusion and structural behaviour

Among the lengthening joints, the "scarfing" method can be further divided in three classes of *scarf*: *halved*, *splayed*, and *bridled*.
A basic *halved scarf*, also called *half-wood* or *half-lap* is probably the simplest to fashion and thus the most abundant to find in structures all over the world. It was usually used in large span structures, in order to enlarge length of beams, tie beams, or protract high columns. It consists in one piece projecting and fitting into the recessed portion of the other. The lap surfaces are parallel with the timbers' and the abutments are shaped with a α right angle. It performs well in axial compression but has moderate shear strength and no bending or tensile strength. A considerable improvement of the basic halved scarf joint is the *halved and undersquinted scarf*. *Halved* refers to the cut of the horizontal surface, that is in correspondence of the half of the timber cross section. *undersquinted* refers to the angle for the abutments, or squints. The angle of the lower squint is not necessarily the same as the angle of the upper one; nevertheless, in the present work the two angles are considered equal and equal to an angle α. Shallower angles increase the likelihood of splitting at the notch, more than bigger angles. This joint is a considerable improvement to the simple *halved* one, because the undersquinted end improves bending strength and resistance to seasoning twist of the joint [16]. The pieces can be assembled together with modern mechanical fasteners (screw, bolts), or traditionally with wooden pegs to improve torsion resistance and resist to tension loads. In the present work the analysis of the effectiveness of the mechanical fastener is decided to be neglected because they are considered as a reinforcement for the joint. It is in fact demonstrated [9] that the effectiveness of the wooden pegs improve the general performances of the joint, but is not necessary for the effectiveness of the specimen. Furthermore, the failure of each of the tested scarf joints demonstrated that the first failure mode of the timber was the shear/failure in the point B (cleavage) instead the shear failure of the pegs, since the cleavage of the timber required less energy than shearing the pegs.
Once excluded the analysis of the presence of mechanical fasteners, the basic load transmission mechanism among the member is via contact pressure and friction on the notches and contact surfaces. Eccentricities caused by the imperfect geometry brings to an irregular and eccentric distribution of forces. This conditions, are neglected for the developing of the analytic models and the basic hypotheses under which this work is developed are: Hp1: compression force between the joint's surfaces; Hp2: presence of friction force for the transmission of the loads; Hp3: perfect adherence between the surfaces. The imperfections are considered as parameters of study and inserted later on in the mechanical model of the structure the joint is part of. The friction is also taken into account for chosen loading conditions and failure modes.

2.2 Experimental campaign and static models.

The present study examines the behaviour of the *halved and undersquinted scarf* under pure compression, pure bending and combined compressive and bending load. In the paper, some laboratory tests are presented as the evidence and the basis for the development of different analytic models.
During the laboratory tests was observed that the along the loading process the connection showed a non-linear-geometric behaviour. However, that non-linear behaviour can be simplified in a sequence of static models where in different loading-instants the position of such resultant forces is described through proper parameters. This phenomena is commented in [14] and further analysed in the following paragraphs.

3 ANALYTICAL CHARACTERIZATION OF THE *HALVED AND UNDERSQUINTED SCARF.*

3.1 The analytic models

In the present section, two analytic models are described. The model (ii) (Fig. 3a) describes the configuration with the generic angle α, where the influence of the static friction μ_α on the surface AB, influent for the earlier stages of the loading process (small force F and small bending moment M), is considered. The model (vii)

(Fig. 3b) describes the configuration where the contribution of the friction force is negligible due to the "reinforcing effect" of the compression force.

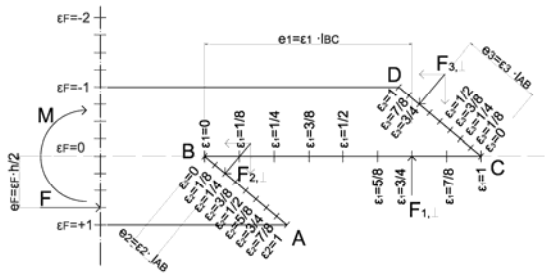

Figure 2. *Definition of the parameters ε_1, ε_2, ε_3, ε_F.*

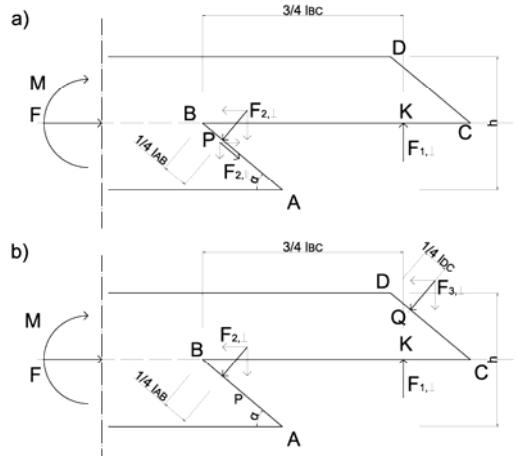

Figure 3. a) *Equilibrium configuration (ii);* ***b)*** *Equilibrium configuration (vii).*

3.2 Model (ii)

Summary of the value of the resultant forces (ii):

$$F_{1,\perp} = F\frac{\cos\alpha + \mu_\alpha \sin\alpha}{\sin\alpha - \mu_\alpha \cos\alpha} \tag{1}$$

$$F_{1,\perp} = \frac{M + F\left[\frac{h}{2}(\varepsilon_F - \varepsilon_2)\right]}{\left[2h\left(\varepsilon_1 - \frac{\varepsilon_2}{4\tan\alpha}\right)\right]} \tag{2}$$

$$F_{2,\perp} = \frac{\cos\alpha}{2\left(\varepsilon_1 - \frac{\varepsilon_2}{4\tan\alpha}\right)}\left\{\frac{M}{h} + 2\cdot F\cdot\left[\tan\alpha\left(\varepsilon_1 - \frac{\varepsilon_2}{4\tan\alpha}\right) + \frac{(\varepsilon_F - \varepsilon_2)}{4}\right]\right\} \tag{3}$$

3.2.1 The compression force on all the surfaces

The inequality

$$F_{1,\perp} \geq 0 \tag{4}$$

describes the limit of validity of the static model (ii) according with the basic hypothesis of compression on the joint's AB surface. At the same time, this boundary condition describes the range of values that μ_α assumes in the correspondent model.

$$S1: \quad \tan\alpha > \mu_\alpha \geq -\frac{1}{\tan\alpha} \tag{5}$$

As a further condition, both the (4) and (5) give a definition of $F_{1,\perp}$. From the equivalence, the equilibrium condition (6) is obtained.

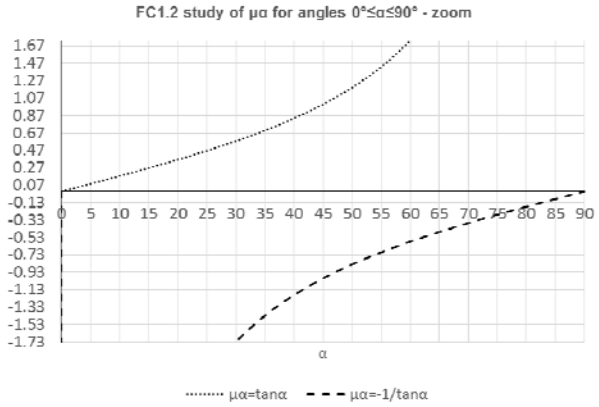

Figure 4. *FC1.2 study of μα for angles 0°≤α≤90°.*

LS1(ii): $f(\mu_\alpha;\varepsilon_1;\varepsilon_2;\varepsilon_3;\varepsilon_F;F;M)$:

$$F = \frac{\frac{M}{h}}{\left[2\left(\varepsilon_1 - \frac{\varepsilon_2}{4\tan\alpha}\right)\left(\frac{\cos\alpha + \mu_\alpha \sin\alpha}{\sin\alpha - \mu_\alpha \cos\alpha}\right) - \frac{(\varepsilon_F - \varepsilon_2)}{2}\right]} \tag{6}$$

The equilibrium equation (6) describes the equilibrium path followed by the specimen along the loading process, until failure.

3.2.2 The parameter μ_α

The static friction force μ_α results from the two facing surfaces AB being pressed together closely; it is thus the force exerted by the surface that makes an effort to move across it. The maximum amount of friction force that a surface can exert is

$$F_{2,\perp} \cdot \mu_\alpha = F_{2,//} \tag{7}$$

The value of friction changes along the loading process. As it will be demonstrate, friction depends upon the nature of the two surfaces and upon the degree to which they are pressed together. According to (ii) it is defined as:

$$\mu_\alpha = \frac{F_{1,\perp}\sin\alpha - F\cos\alpha}{F\sin\alpha + F_{1,\perp}\cos\alpha} \tag{8}$$

The friction force is a parameter that depends on the angle α of the squint. The value of initial friction, in case of pure bending loading, is:

$$\mu_\alpha = \tan\alpha \tag{9}$$

This initial value, depending only on geometric variables, decreases up to the value of $\mu_\alpha = 0$, correspondent to the $F_{2,//} = 0$. The change of direction of the vector force $F_{2,//}$, together with the increased values of *F*, maintain the joint's laps together. The detailed description of the importance of the understanding of the μ_α is later demonstrated with experimental evidence.

3.2.3 Failure modes

The failure modes (FM) are three and are following described as:

II. Shear/tension perpendicular to the grain failure in the point B.
III. Combined shear/tension perpendicular to the grain failure in the point B and C.
IV. Buckling.

3.2.4 Limit states

The static models provide limit states (LS) that reflect the three failure modes observed during the experimental campaign:

- **LS1:** equilibrium limit state. It is described by the equilibrium equation (6). Critical parameters that bring to the failure are geometric parameters.
- **LS2** and **LS3**: limit states associated with the failure mode shear/tension perpendicular to the grain. The failure modes associated with the LS2 and LS3 are respectively the FM II and FM III. The critical parameters that bring to the failure are the strength and stiffness of the material and geometric parameters.

LS1(ii)

The equation (6) describes the limit state or equilibrium state LS1. This equilibrium equation describes the loading path of the specimen demonstrated in the paragraph 5.2. More, in the particular case $\mu_\alpha = 0$ is verified:

$$\frac{M}{h} = 2F\left[\frac{1}{\tan\alpha}\left(\varepsilon_1 - \frac{\varepsilon_2}{4\tan\alpha}\right) - \frac{(\varepsilon_F - \varepsilon_2)}{4}\right] \tag{10}$$

LS2(ii)

$$F_{1,\perp} \le F_f \tag{11}$$

$$F \le \frac{2}{(\varepsilon_F - \varepsilon_2)}\left[2 \cdot F_{f\cdot}\left(\varepsilon_1 - \frac{\varepsilon_2}{4\tan\alpha}\right) - \frac{M}{h}\right] \tag{12}$$

In the LS2, it is contained the information about the position of the point of application of the resultant forces $F_{2,\perp}$ and $F_{1,\perp}$. It is clear how the position of these two forces are of basic importance for the description of the load bearing capacity of the connection. With the changing of position of the parameter ε_1 or ε_2 (Fig. 2) the load bearing capacity of the joint increases [14].

LS3(ii)

In the LS3, the basic information is the value of static friction μ_α and the amount of applied external force F.

$$F_{1,\perp} = F\frac{\cos\alpha + \mu_\alpha \sin\alpha}{\sin\alpha - \mu_\alpha \cos\alpha} \le F_f \tag{13}$$

$$F\frac{\cos\alpha + \mu_\alpha \sin\alpha}{\sin\alpha - \mu_\alpha \cos\alpha} \le F_f \tag{14}$$

In this case the load bearing behaviour is determined by the inclination of the squint and the consequent friction coefficient.

The latter two failure modes refer to the value $F_f = F_u$, that is the maximum value that the force F can assume. The F_f, value of the force that is necessary to start the failure in a cracked beam, is defined by [8]. Basic information and the significance of F_f are analysed in the section 5 of the present work.

3.3 Model (vii)

Summary of the value of the resultant forces (vii):

$$F_{1,\perp} = \frac{F}{\tan\alpha} \tag{15}$$

$$F_{2,\perp} = F\left\{\frac{1}{\sin\alpha} - \frac{\left[\frac{(\varepsilon_2 - \varepsilon_F)}{4} + \frac{1}{\tan\alpha}\left(\varepsilon_1 - \frac{\varepsilon_2}{4\tan\alpha}\right)\right]}{\left(\cos\alpha - \frac{\varepsilon_2 + \varepsilon_3}{4\sin\alpha}\right)}\right\} + \frac{\frac{M}{2h}}{\left(\cos\alpha - \frac{\varepsilon_2 + \varepsilon_3}{4\sin\alpha}\right)} \tag{16}$$

$$F_{3,\perp} = \left\{F\left[-\frac{(\varepsilon_F - \varepsilon_2)}{4} + \frac{1}{\tan\alpha}\left(\varepsilon_1 - \frac{\varepsilon_2}{4\tan\alpha}\right)\right] - \frac{M}{2h}\right\}\frac{1}{\left(\cos\alpha - \frac{\varepsilon_2 + \varepsilon_3}{4\sin\alpha}\right)} \tag{17}$$

3.3.1 Limit case (vii) = (ii)

This limit case demonstrate the consequential order of the two models (ii) and (vii). The equilibrium condition (10) for (ii) in case $\mu_\alpha = 0$ is in fact verified for the model (vii) in the case

$$F_{3,\perp} = 0 \tag{18}$$

3.3.2 Failure modes

The expected failure modes identified for the model (vii) are mainly 2:

I. Compression inclined to the fibers in the surface CD
II. Shear/tension perpendicular to the grain failure in the point B.
III. Combined shear/tension perpendicular to the grain failure in the point B and C.

The failure I, expected during the elaboration of the analytical model, was later on discarded without counterpart in the experimental campaign.

3.3.3 Limit states

The static model provide one limit state that reflect the failure modes FM II and FM III registered during the experimental campaign. The LS4 depends on strength and stiffness of the material and geometric parameters.

3.3.4 LS4 (vii):

For the fracture in B

$$F_{2,\perp} \cdot \cos\alpha \le F_{f,2} \tag{19}$$

For the fracture in C:

$$F_{3,\perp} \cdot \cos\alpha \le F_{f,3} \tag{20}$$

The analytic evaluation of the FM II and FM III is done according with the Gustafsson formula of the energy of failure. The parameter a_i is evaluate as follows:

- failure in B, FM III:

$F_{f,2}(a_2)$: (21)

$$a_2 = e_2 \cdot \cos\alpha = \varepsilon_2 \cdot l_{AB} \cdot \cos\alpha = \varepsilon_2 \cdot \frac{h}{2 \cdot \sin\alpha} \cdot \cos\alpha = \varepsilon_2 \cdot \frac{h}{2 \cdot \tan\alpha}$$

- failure in C, FM III:

$F_{f,3}(a_3)$: (22)

$$a_3 = e_3 \cdot \cos\alpha = \varepsilon_3 \cdot l_{CD} \cdot \cos\alpha = \varepsilon_3 \cdot \frac{h}{2 \cdot \sin\alpha} \cdot \cos\alpha = \varepsilon_3 \cdot \frac{h}{2 \cdot \tan\alpha}$$

The failure mode FM III fracture in C is evaluated changing the direction of the bending moment *M*, thus the fibers in C belongs to the second half of the specimen. The adopted formula is thus the (23).

$$F \le \left\{ F_{f,3} + \frac{(-M)}{2h} \frac{\cos\alpha}{\left(\cos\alpha - \frac{\varepsilon_2+\varepsilon_3}{4\sin\alpha}\right)} \right\} \frac{\left(\cos\alpha - \frac{\varepsilon_2+\varepsilon_3}{4\sin\alpha}\right)}{\cos\alpha\left[\frac{(\varepsilon_2-\varepsilon_F)}{4} + \frac{1}{\tan\alpha}\left(\varepsilon_1 - \frac{\varepsilon_2}{4\tan\alpha}\right)\right]} \quad (23)$$

4 EXPERIMENTAL CHARACTERIZATION OF THE *HALVED AND UNDERSQUINTED SCARF*

4.1 Material and methods

The specimen are prepared from artificially dried solid timber beams of 6.5 m of length with a cross-section of b = 60 mm h = 140 mm. The wood specie is *Picea abies* (Spruce) of timber class C24. The specimens are stored at a temperature of t = 20° C and a relative humidity of 65%. The following table summarizes some of the samples with the respective properties [13].

Table 1: *moisture content, density and average ring width of the specimen (from [13]).*

Geometry	Moisture content [%]	Density [kg/m³]	Average ring width [mm]
α = 45°	16.5	422.4	2.4
α = 30°	17.1	512.3	1.9

The properties used for the analytic calculations are the ones contained in the EN 338:2002 and EN 1912:2004 for the timber class C24.

The Figure 5 represents the specimen. The facing adjacent surfaces are in contact. The peaks in correspondence with points B and C are cut-away to avoid the split-effect that can anticipate the failure. The two considered angles for the squints are α = 30° and α = 60°.

The test machine used is the combination of two subsystems, two hydraulic jacks, one for vertical loads and the other for the horizontal loads. The pistons move respectively vertically up and down (F_I) and left-right (F_{II}) in a linear guide. The Piston I is used for the application of axial forces ($F_{applied} = F_I$) and the Piston II for the application of bending moment ($F_{applied} = F_{II}$). The force is exerted on the test specimen by means of movable cross-heads fixed to the fixed frame. The head of the Piston II is provided with a head for the application of bending moment to the specimen. The applied test procedures are two.

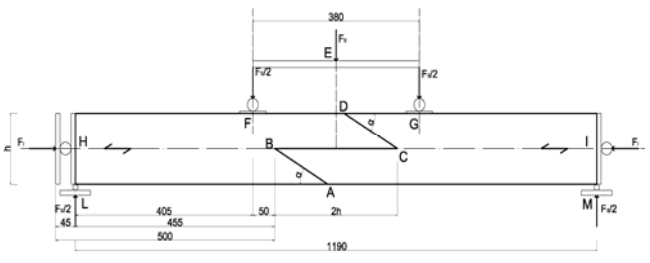

Figure 5: *Test installation of the specimen*

4.1.1 PROCEDURE 1 (P1)

The application of the load according to P1 is described by the separate and consecutive loading of the specimen by means of the Piston I and Piston II. Both pistons work with load or stress-controlled mode.

The relation among the applied F_{II} force and the bending moment M and the relation among the applied F_I force and the normal force N are defined by the following (24) and (25).

$$N = F_I \quad (24)$$

$$M = \frac{F_{II}}{2}\overline{FH} \quad (25)$$

In the P1, an interesting phenomena described as *passive response* on the Piston II and Piston I was registered. The *passive response* consists in the presence of a *passive* force F on the inactive piston. Following two cases are described.

a) The activation of the force F_{II} causes the passive response $F_{I,passive}$ ($F_{I,passive} = F_I$) on the Piston I. Referring to the Figure 6, the specimen is restrained along the axial direction at the two extremities H and I. During the application of the load F_{II}, the joint rotates; therefore, because of its geometry, the two connected elements separate one from the other, and both the far ends displace along the direction of the beam's axis. This deformation provokes the passive $F_{I,passive}$ compression load. The behaviour depends on the chosen α.

b) Similarly, the activation of the force F_I on the Piston I causes the passive response $F_{II,passive}$ ($F_{IIpassive} = F_{II}$) on the Piston II. Referring to the Figure 7, the specimen is restrained because of the presence of the Piston II. During the application of the load F_I, because of its geometry, the joint rotates; the central part of the connected elements bent in the direction of the Piston II and activate the passive $F_{II,passive}$ compression.

This tests performed with P1 are the simulation of a jointed beam in a real on-site-jointed-beam. The surrounding structure is in fact a restraint for the displacement/rotation of the beam.

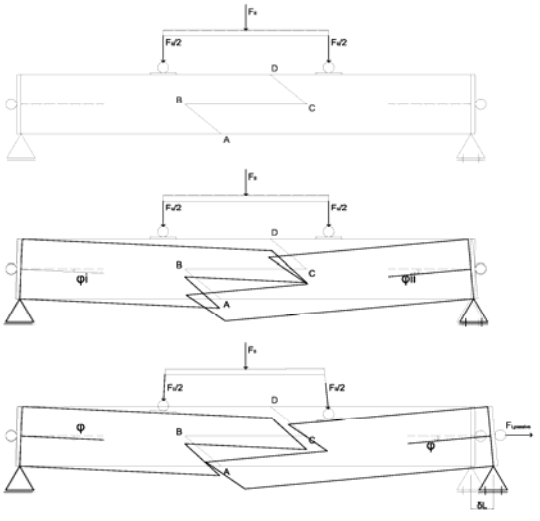

Figure 6: *Passive response of the Piston I*

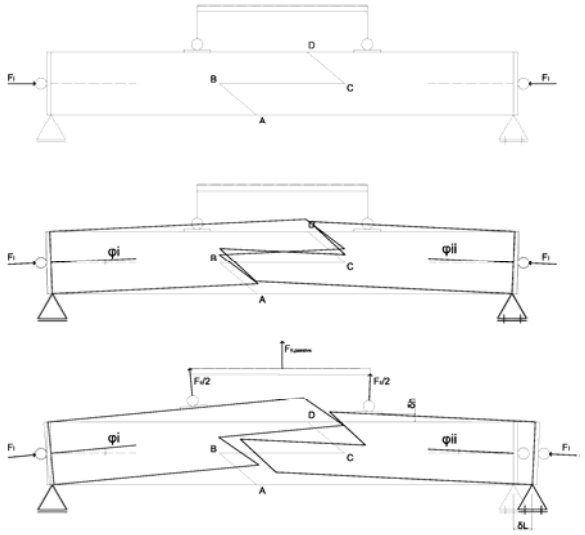

Figure 7: *Passive response of the Piston II.*

4.1.2 PROCEDURE 2 (P2)

The tests performed with PROCEDURE 2 are mixed force-controlled and displacement-controlled mode. The P2 is described by the separate and consecutive loading of the specimen by means of the Piston I and Piston II. The load F_I increases with force-controlled mode up to the chosen value of F_{target} afterwards, the F_{II} with displacement-controlled mode is applied until the failure of the specimen. The hydraulic jack constantly adjusts the specific ultimate target F (F_{target}).

The relation among the applied F_{II} force and the bending moment M and the relation among the applied F_I force and the normal force N are defined by the following equation (24) and (25).

4.2 Test results

In following Figure 8 and Figure 9 a summary of the behaviour of the test results for the *halved splayed scarf* with squint α = 30° and α = 60° is given. The Table 1 contains the description of the test results of the mentioned diagrams, performed with both the procedure P1 and P2, where the comparable data are highlighted.

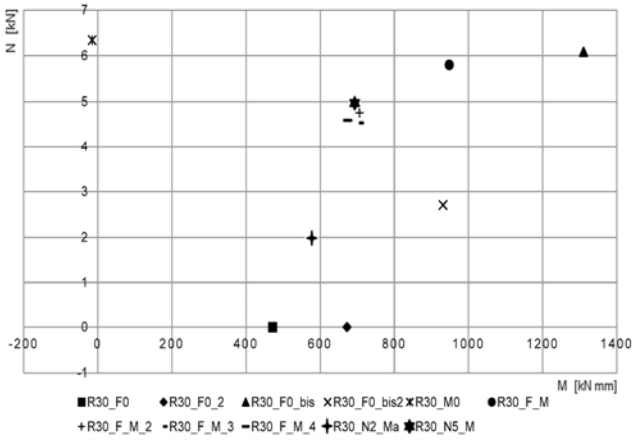

Figure 8: *N-M interaction curve for α = 30°*

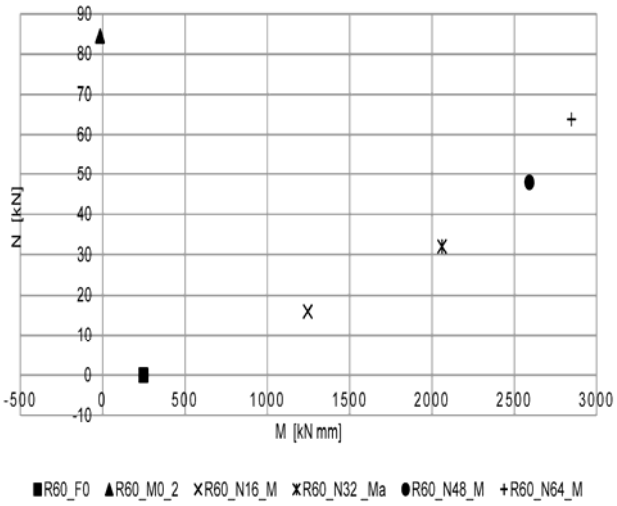

Figure 9: *N-M interaction curve for α = 60°*

Table 2: *Experimental data and failure modes of the specimens*

Procedure	M_u [kN mm]	F_u [kN]	F_{target} [kN]	Specimen	Note
α = 30°					
P1a	470.61	0	-	R30_F0	FM shear/tension B
P1a			-	R30_F0_2	FM shear/tension B. Same
P1c	1345.8	6.41	-	R30_F0_bis	FM shear/tension B
P1c	879.46	7.87	-	R30_F0_bis2	FM shear/tension B
P1d	0	8.4	-	R30_M0	FM shear/tension B+C
P1c	992.66	6.17	-	R30_F_M	FM shear/tension B
P1b	4.78 (s)	5.48 (s)	1	R30_F_M_2	Stop first crack. Same
P1b	4.78 (s)	5.48 (s)	0.5	R30_F_M_3	Stop first crack. Same
P1b	4.78 (s)	5.48 (s)	0.25	R30_F_M_4	Stop first crack. Same
P2	580.37	1.98	2	R30_N2_Ma	FM shear/tension B
P2	516.98	1.98	5	R30_N5_M	FM shear/tension B
α = 60°					
P1a	247.65	0	-	R60_F0	FM instability
P1d	-15.99	42.00 (s)	-	R60_M0	Stopped, instability
P1d	-15.39	84.51 (s)	-	R60_M0_2	Stopped, instability
P2	1244.16	16	16	R60_N16_M	FM shear/tension B
P2	2069.34	32.06	32	R60_N32_Ma	FM shear/tension B
P2	2601.72	47.96	48	R60_N48_M	FM shear/tension B, critic crack points also ε1=1/4 and ε3=1/4
P2	3063.82	63.97	64	R60_N64_M	Test interrupted for bending of the upper plate, danger instab.
KEY:					
	Comparable procedures				
(s)	Stopped test (not up to break)				

4.3 Failure modes

From the test, three different failure modes (FM) are identified:

I. Shear/tension perpendicular to the grain failure in the point B
II. Combined shear/tension perpendicular to the grain failure in the point B and C
III. Buckling

The FM II is showed for small and big angles (Figure 10a and Figure 10b); while the FM III for only small angles (Figure 10c) and the FM IV for only big angles (Figure 10d and Figure 10e).

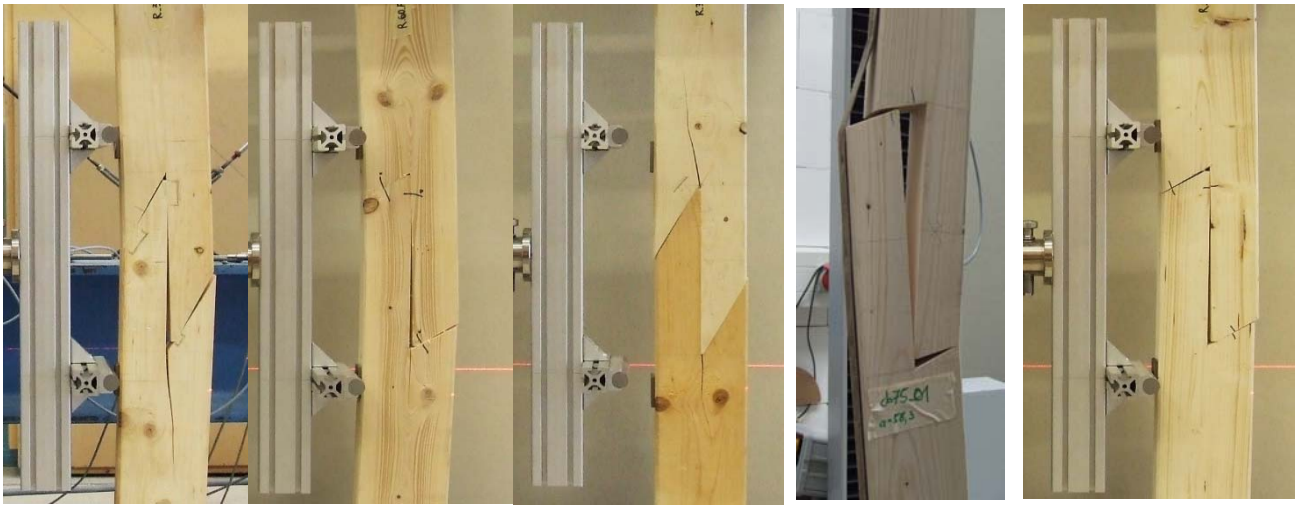

(a) (b) (c) (d) (e)

Figure 10: *(a): Specimen R30_F0 α=30° 20/01/2016 pure bending. FM II; (b): Specimen R60_F64_M α=60° 01/02/2016 bending + compression. FM II; (c): Specimen R30_M0 α=30° 20/01/2016 - pure compression. FM III; (d): Specimen α= 75° compression + bending a=58,3 05/06/2015. FM IV; (e): Specimen R60_F0 α= 60 pure bending. FM IV.*

4.4 Conclusions

Considering the general behaviour of the *halved splayed and scarf joint*, it is not possible to do a general description of the joint's behaviour only dependent on the ratio F/M; in fact, the differences in the behaviour of the joint, from the loading response, to the failure modes are remarkable in dependence of the joint geometry.
The inclination of the squint influences:

- The failure mode;
- The load-bearing capacity.

The loading process is described through N-M diagram. In the diagram, depending on the loading conditions, three main failure-areas are identified. These three areas have "shifting boundaries" depending, first, on the geometry of the joint, second, on the kind of stressing loads, third, the positioning of the external forces respect to the correspondent geometry. For the specimen with small angles and big angles, represented respectively by the performed tests with α = 30° and α = 60°, the failure modes are schematised in details in the Figure 11.
For what concern the α = 30°, the area that corresponds to the FM II correspond approximately to the big majority of the N-M diagram, corresponding to a value of applied normal force $F_I = 0.88 \cdot F_u$; in fact, the FM III is achieved only by specimens loaded in pure compression. For the small angles, the buckling failure was not registered.
For what concern the α = 60°, in the lower area of the diagram, correspondent to pure bending and combined bending and compressive force up to a value of $F_I = 0.2 \cdot F_{ue}$, the buckling (FM IV) failure was prevalent. From a value of $0.2 \cdot F_{ue} \leq F_I < F_{ue}$ the prevalent failure is the FM II. For specimens α = 60° was not experimentally possible to get values $F_I > F_{ue}$. F_{ue} is not the real limit value F_u for pure compression, but it corresponds to F_{ue} = 80 kN, the maximum value we obtain from the machine, for safety reasons. The failure mode for values of $F_I \geq F_{ue}$, is hypothesized to be the FM III and then the FM IV.

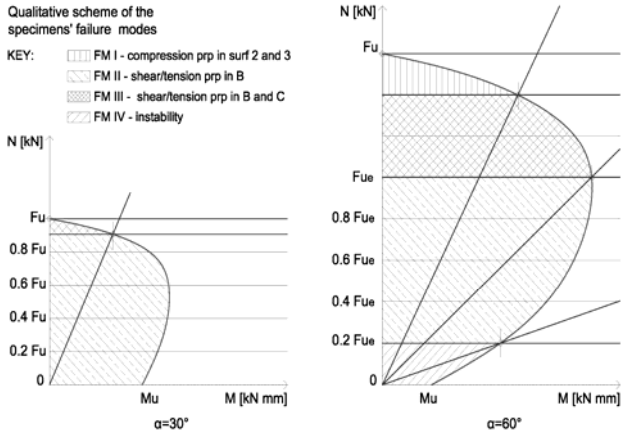

Figure 11: *Qualitative schema of the specimen's failure mode for α = 30° and α = 60° (qualitative scale of the diagrams).*

5 Experimental significance of the parameters contained in the analytical models

5.1 Variation of the ε_1 along the loading process for different α

The general behaviour of the joint was furthermore completed with some test to determinate the precise value of the parameters ε_1, ε_2, ε_3 (Fig. 2) along the loading process. The passage from the zero load to the ultimate-load showed then a non-linear behaviour of the connection; in fact, is observed that the length of the segments AB, BC and CD reduces in dependence of the increasing compression/bending load (Figures 12a, b, c). To describe the change of position in the resultant forces, $F_{1,\perp}$, $F_{2,\perp}$, $F_{3,\perp}$ along the loading process, consecutive configurations for ε_1, ε_2, ε_3 are defined. The medium values are defined in Table 3 for both groups of specimens α = 30° and α = 60°.

Table 3. *Medium values for the parameters ε_1, ε_2, ε_3 in the tests α=30°specimen R30_M0 and R30_F0_bis_2 and in the tests α=60° specimen R60_F0 and R60_F16_M.*

	Active F_{II} (Model (ii))			Active F_I (Model (vii))		
α=30°						
F_u values	**ε1**	**ε2**	**ε3**	**ε1**	**ε2**	**ε3**
0Fu	1/2	1/2	1/2	1/2	3/4	1/4
0,2Fu	3/4	3/16	5/8	1/2	3/4	1/4
0,4Fu	13/16	3/16	13/16	5/8	1/2	3/16
0,6Fu	7/8	1/8	7/8	3/4	1/2	3/16
0,8Fu	7/8	1/8	7/8	7/8	1/2	1/8
Fu	15/16	1/8	7/8	7/8	1/2	1/8
α=60°						
0Fu	7/8	1/2	1/2	1/2	1/2	1/2
0,2Fu	7/8	1/2	1/2	1/2	1/2	1/2
0,4Fu	7/8	3/8	5/8	1/2	1/2	1/2
0,6Fu	15/16	3/8	5/8	1/2	1/2	1/2
0,8Fu	15/16	1/4	3/4	1/2	1/2	1/2
Fu	15/16	1/4	13/16	(Fue) 1/2	(Fue) 1/2	(Fue) 1/2

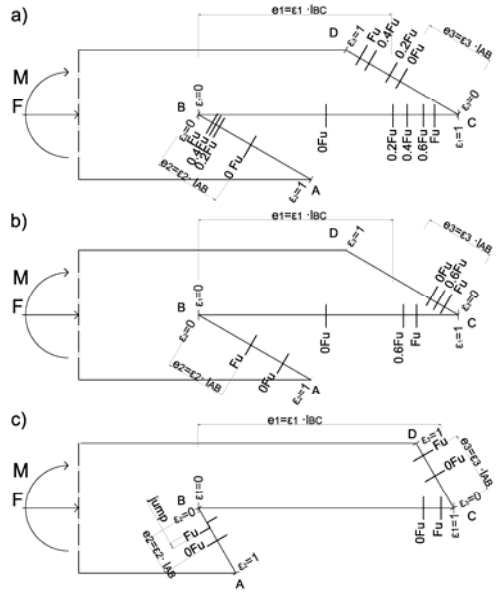

Figure 12: **a)** *Specimen R30_F0_bis_2 (α = 30°; F_{II}). Positioning of the resultant force along the loading process;* **b)** *Specimen R30_M0 (α = 30°; pure compression). Positioning of the resultant force along the loading process;* **c)** *Specimens R60_F0 (α = 60°; pure bending) and R60_F16_M (α = 60°; F_I (=16kN)+ F_{II}). Positioning of the resultant force along the loading process.*

The specimens α = 30° and α = 60° behave differently. On one side, the α = 30° shows very evident changes in the resultant forces' positions along the loading process; but, with the contemporary deformation (continuous adherence) of the two joint's left and right branches.
On the other hand, the α = 60° specimens show a zero load configuration very close to the F_u configuration. Nevertheless, in the case of low values of F_I (in the order of $F_I = 0.6 \cdot F_u$) and presence of bending load, the FM IV is registered. The surface AB slips on the adjacent surface. The "jump" of the right piece on the left piece of the specimen in correspondence of a load stress equal to Fu is represented in the Figure 12c, in red. On the other side, the specimen α = 60° in case of pure compression:

- maintain until F_{ue} a perfect adherence among the adjacent surfaces;
- the resultant force are centered on all the surfaces for a value of load $0 < F \leq F_{ue}$.

5.2 Verification of the μ_α parameter

The data in the Table 4 describe the model R30_F0_bis, performed with procedure P1-b. For any of the pair of forces recorded in different loading instants, the value of the resultant forces and friction according with the analytical model (ii) are described. The values of ε_1, ε_2, ε_3 accord with the values observed in Table 3. The values of friction described in the Table 4 and represented in the Figure 13, demonstrate that along the loading process, the connection follows the values of μ_α expected for the (5).

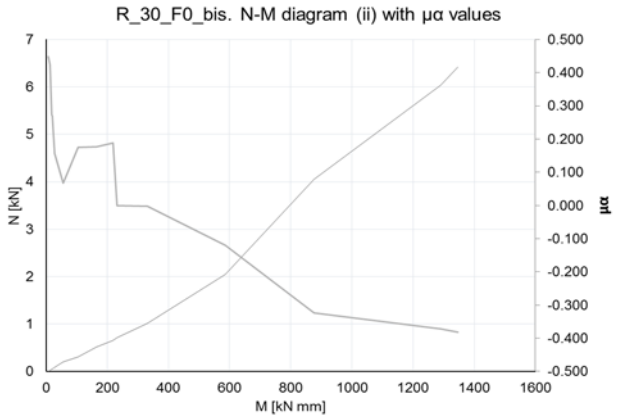

Figure 13. *N-M interaction curve of the test specimen R30_F0_bis with μα values.*

Table 4. *Specimen R30_F0_bis. Data test and analytical elaboration according with (ii)*

		α [°]	h [mm]	ε1	ε2	test results: II piston lever arm	test results: II piston FII [kN]	test results: II piston M [kN mm]	test results: I piston FI=N [kN]	analytic results model (ii): F2,⊥ [kN]	F2,// [kN]	F1,⊥ [kN]	F3,⊥ [kN]	μα
R_30_F0_bis	a	30	140	0.5	0.5	405	0.04	8.1	0.01	0.09	0.04	0.098	-	0.448
	b	30	140	0.5	0.5	405	0.06	12.5	0.018	0.135	0.057	0.145	-	0.423
	c	30	140	0.5	0.25	405	0.093	18.833	0.056	0.212	0.058	0.213	-	0.272
	d	30	140	0.5	0.25	405	0.134	27.135	0.09	0.247	0.039	0.233	-	0.156
	e	30	140	0.5	0.25	405	0.274	55.485	0.208	0.624	0.042	0.424	-	0.067
	f	30	140	0.5	0.25	405	0.52	105.3	0.312	1.07	0.188	0.855	-	0.175
	g	30	140	0.5	0.25	405	0.813	164.63	0.515	1.486	0.263	1.419	-	0.177
	j	30	140	0.5	0.25	405	1.078	218.3	0.66	1.962	0.371	1.885	-	0.189
	k	30	140	0.75	0.25	405	1.146	232.07	0.707	1.412	-0.001	1.223	-	-0.001
	l	30	140	0.75	0.25	405	1.633	330.68	1.009	2.013	-0.003	1.742	-	-0.001
	m	30	140	0.81	0.19	405	2.897	586.64	2.05	3.392	-0.409	2.734	-	-0.12
	n	30	140	0.88	0.13	405	4.332	877.23	4.057	5.2	-1.682	3.662	-	-0.324
	o	30	140	0.94	0.13	405	6.375	1290.9	6.04	7.355	-2.728	5.006	-	-0.371
	p	30	140	0.94	0.13	405	6.646	1345.8	6.417	7.724	-2.95	5.214	-	-0.382

Furthermore, the test R30_F0_bis verifies the LS1 (ii). Referring to the Table 4, for the selected pair of forces, the verification of the equilibrium condition LS1(ii) follows:
c) M = 18.833; N = 0.005; $\mu_\alpha = 0.534$; $\varepsilon_1 = 0.5$; $\varepsilon_2 = 0.25$.
→ $0.0056 \cong 0.00565$;
j) M = 218.30; N = 0.660; $\mu_\alpha = 0.189$; $\varepsilon_1 = 0.5$; $\varepsilon_2 = 0.25$.
→ $0.66 \cong 0.6599$;
l) M = 330.68; N = 1.00; $\mu_\alpha = -0.001$; $\varepsilon_1 = 0.75$; $\varepsilon_2 = 0.25$.
→ $1.009 \cong 1.008$;

p) M = 1345.8; N = 6.417; μ_α = -0.232; ε_1 = 0.937; ε_2 = 0.125. → 6,417 ≅ 6.417 .

As already observed, the value of friction, is varies along the loading process, and the special value of friction $\mu_\alpha = 0$ is univocally described by (18). For the case k): M = 232.07; N = 0.707; μ_α = -0.001; ε_1 = 0.75; ε_2 = 0. 25. → 232.07 ≅ 232.523 .

The equilibrium conditions (6) describe the equilibrium path of the specimen along the loading process, for a value of load $0 < F \leq F_{ue}$.

5.3 Verification

The prediction of the failure of the *halved and scarfed joint* was not possible through the adopted models; nevertheless, once obtained the experimental results was possible to characterised the load-carrying capacity and other parameters of the specimens thanks to the proposed models (Figure 15).

In the present section, the specimen R30_F_M is described through the limit states LS1, LS2, LS3, LS4. For the LS4, FM III was possible to anticipate the $F_u = F_f$ according with the Gustafsson formula for the evaluation of the energy of propagation of a crack [8]. With the LS1 the description of the friction parameter at the failure was possible, and finally with to the LS3 the experimentally $F_{u,exp}$ is analytically verified. The evaluation of the F_u is experimentally proceeded thanks to the LS2.

LS1:

Thanks to the LS1 (ii) the straight lines of constant μ_α are described as in the Figure 15. In the results' description, the value of μ_α for the single specimen is evaluated through the failure values F_u and M_u contained in the Table 2. The specimens are ordered along the correspondent straight line's values of μ_α on the diagram.

LS2 (FM II):

The analytical values of $F_{f,analy}$ for the specimens are calculated according with the Gustafsson formula of the energy of failure. In case of fracture in B, the formula is (25):

$$F_{f,2,analy} \cong \sqrt{G_f \cdot b \cdot \frac{E_0 \cdot J}{a_2^{\,2}}} = \sqrt{G_f \cdot b \cdot \left(\frac{b \cdot h_{eff}^3}{12}\right) E_0 \cdot \frac{1}{a_2^{\,2}}} \tag{25}$$

where the parameter a_2 is evaluate as (21).

The experimental evaluation of the $F_{f,2}$ for the FM II is done starting from the experimental results contained in the Table 2 inserted the LS2 (ii) (11).

For the specimen R30_F_M the following analytic (26) and experimental results (z) follow.

$$F_{f,2,analy} = 19.38\,kN \tag{26}$$

$$F_{f,2,analy} = 4.92\,kN \tag{27}$$

In the Figure 16 is thus represented the straight line of constant F_f for the specimen R30_F_M the analytic result is $F_{f,3,analy}$ = 5 kN.

LS3:

Finally, the LS3 describes the F_u for the single specimen, considering (except the pure compression load):

1. μ_α = experimental value evaluated according with LS1(ii)
2. $F_{f,exp}$ = experimental value calculated according with LS2(ii)

For the specimen R30_F_M, fixed value of $F_{f,exp} = 5$ for the value of $\alpha = -0.393$, the value of F_u is verified through the (14) LS3(ii):

$$F_u = F_f \frac{\sin\alpha - \mu_\alpha \cos\alpha}{\cos\alpha + \mu_\alpha \sin\alpha} \tag{28}$$

LS4 (FM III):

For the analytic values of $F_{f,analy}$ for the FM III in the specimens are also calculated according with the Gustafsson formula of the energy of failure. The $F_{f,2}$ for the fracture in B is calculated in (25), while for the fracture in C is valid the following (29).

$$F_{f,3,analy} \cong \sqrt{G_f \cdot b \cdot \frac{E_0 \cdot J}{a_3^{\,2}}} = \sqrt{G_f \cdot b \cdot \left(\frac{b \cdot h_{eff}^3}{12}\right) E_0 \cdot \frac{1}{a_3^{\,2}}} \tag{29}$$

where the parameter a_3 is evaluate as (22).

The experimental evaluation of the $F_{f,exp}$ for the FM III is done starting from the experimental results F_u and M_u contained in the Table 2 inserted in the (23) for LS4(vii).

$$F_{f,3,\exp} = 8\,kN \tag{30}$$

The following Figure 14 reflect both the analytical and experimental evaluation of the FM III (vii).

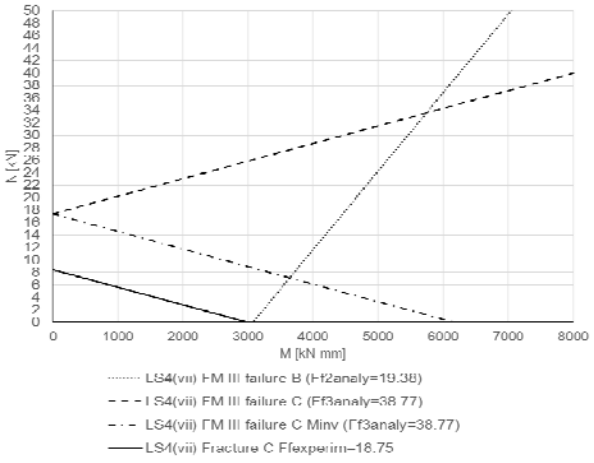

Figure 14. *Analytical evaluation of the FM III (vii) for α = 30°.*

On one side, the $F_{f,2,analy}$ is not reflecting the experimental results, on the other side the $F_{f,3,analy}$ is in the range of the experimental results $F_{f,exp}$ calculated back from the test results. The failure mode FM III fracture in C is evaluated with (23).

In the following Figure 16 the test results for the α = 30° R30_F_M are described according with the parameters evaluated thanks to the analytical models (ii) ad (vii). For

all the other specimen the respective values of μ_α, $F_{f,exp}$ are given.

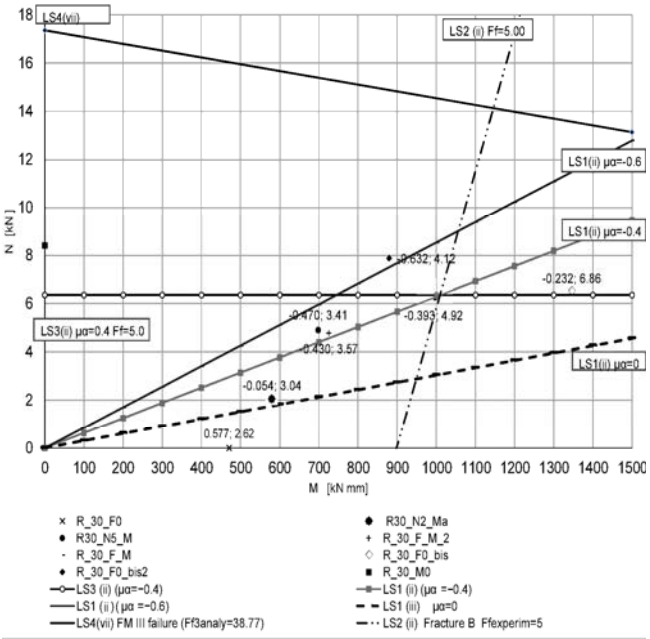

Figure 15: *F-M(α=30°) – Example of description of the test specimen F30_F_M. Data description: μα ; Ff.*

6 CONCLUSIONS

The description of such carpentry connection through a static model is of importance in a scientific field for the knowledge of the mechanical behaviour of old constructional systems and many applications in the structural analysis with the aim of reinforce and restoration of old timber structures.

It is evident that the possibility to describe the failure mode of the *halved splayed scarf* through this static model is possible, but the prediction of the ultimate force F_u is not possible, without considering the variation of all the parameters. Furthermore, the Gustafsson formula used for the description of the *notched joint* in the Eurocode and the original formula, do not suit the tension perpendicular to the grain that is observed for the *halved splayed scarf*.

As an outlook, more research is needed:

- in order to have a non-linear description of the joint;
- in order to develop a theory that permit the description of the fracture of an acute-notch angle where is the contemporary action of the two forces with opposite verse applied on the two sides of the angle that causes tension perpendicular to the grain.

ACKNOWLEDGEMENTS

I thank the Labor für Holztechnik der Fakultät Bauen und Erhalten in the HAWK Hildesheim and their technicians for their availability and punctuality in performing the test.

REFERENCES

[1] Aira J. R., Arriaga F., Íñiguez-González G., Guaita M.. Failure modes in halved and tabled tennoned timber scarf joint by tension test. In: *Construction and Building materials* 96 (2015) pages 360-367.

[2] Blass H. J., Aune P. et alii., *Timber Engineering, STEP 1, Basis of design, material properties , structural components and joints*, Centrum Hout, Netherlands, 1995.

[3] Branco J. M., Descamps T.. Analysis and strengthening of carpentry joints. In: *Construction and Building Materials* 97 (2015) pages. 34–47.

[4] C.T.E., Documento Básico SEM. Seguridad estructural – Estructuras de madera. A código técnico de la edificación, ministerio de viviendal 2006.

[5] DIN 1052, Entwurf, Berechnung und Bemessung von Holzbauwerk. Allgemeine bemessungsregeln und bemessungsregeln fur den hochbau; 2004.

[6] DIN EN 1995-1:2005, NCI NA 6.8.3. National German Annex to Eurocode 5: design of timber structures. Part 1–1. Common rules and rules for buildings. Brussels: CEN, European Committee for Standardization; 2005.

[7] Eurocode 5, *Design of timber structures* - Part 1-1: General – Common rules and rules for buildings. EN 1995-1-1:2004.

[8] Gustafsson P.. Fracture perpendicular to Grain – Structural applications. In: Thelandersson and Larsen H., J., *Timber Engineering*, Wiley, 2003.

[9] Hirst, E., Brett, A., Thomson, A., Walker, P. and Harris, R.. The structural performance of traditional oak tension and scarf joints. In: *10th WCTE, 2008-06-02 - 2008-06-05*, Miyazaki, Japan, 2008.

[10] Kessel M., Augustin R.. Load behaviour of Connections with Pegs II, *Timber Framing*. 39 (3/1996) pages 8-11.

[11] Kessel M., Augustin R.. Load behaviour of Connections with Pegs, *Timber Framing*. 38 (12/1995) pages 6-9.

[12] Larsen, H. J. and Gustafsson, P. J.. 1990. The fracture energy of wood in tension perpendicular to the grain – results from a testing project. In: *Proc. of CIB-W18A Meeting 2*3, Lisbon, Portugal. Paper No. CIBW18/23-19-2.

[13] Otten, J. B.. *Experimentelle und analytische Untersuchung auf Tragfähigkeit und Gebrauchstauglichkeit des beidseitig schräg eingeschnittenen Geraden Blattes*, Unpublished bachelor thesis, HAWK, Hildesheim, Germany, 2015.

[14] Perria, E., Paradiso M., Kessel M.. (2016) Experimental verification of the static model for the characterization of the halved and undersquinted scarf connection. In: *Proc. of 10th International Conference on Structural Analysis of Historical Constructions*, Leuven, Belgium.

[15] Sangree R. H., Schafer B.W.. Experimental and numerical analysis of a stop-splayed traditional timber scarf joint with key. In: *Construction and Building materials* 23 (2009) pages 376-385.

[16] Sobon J. A. *Historic American Timber Joinery: A Graphic Guide*, Pub. By Timber Framers Guild, Ed. by Kenneth Rower, 2002.

[17] Yeomans D. T., Repairs to Historic timber structures: Changing attitudes and knowledge. In: *Structural analysis of historic construction* (eds D'ayala & Fodde), Taylor and Francis, London, 2008.